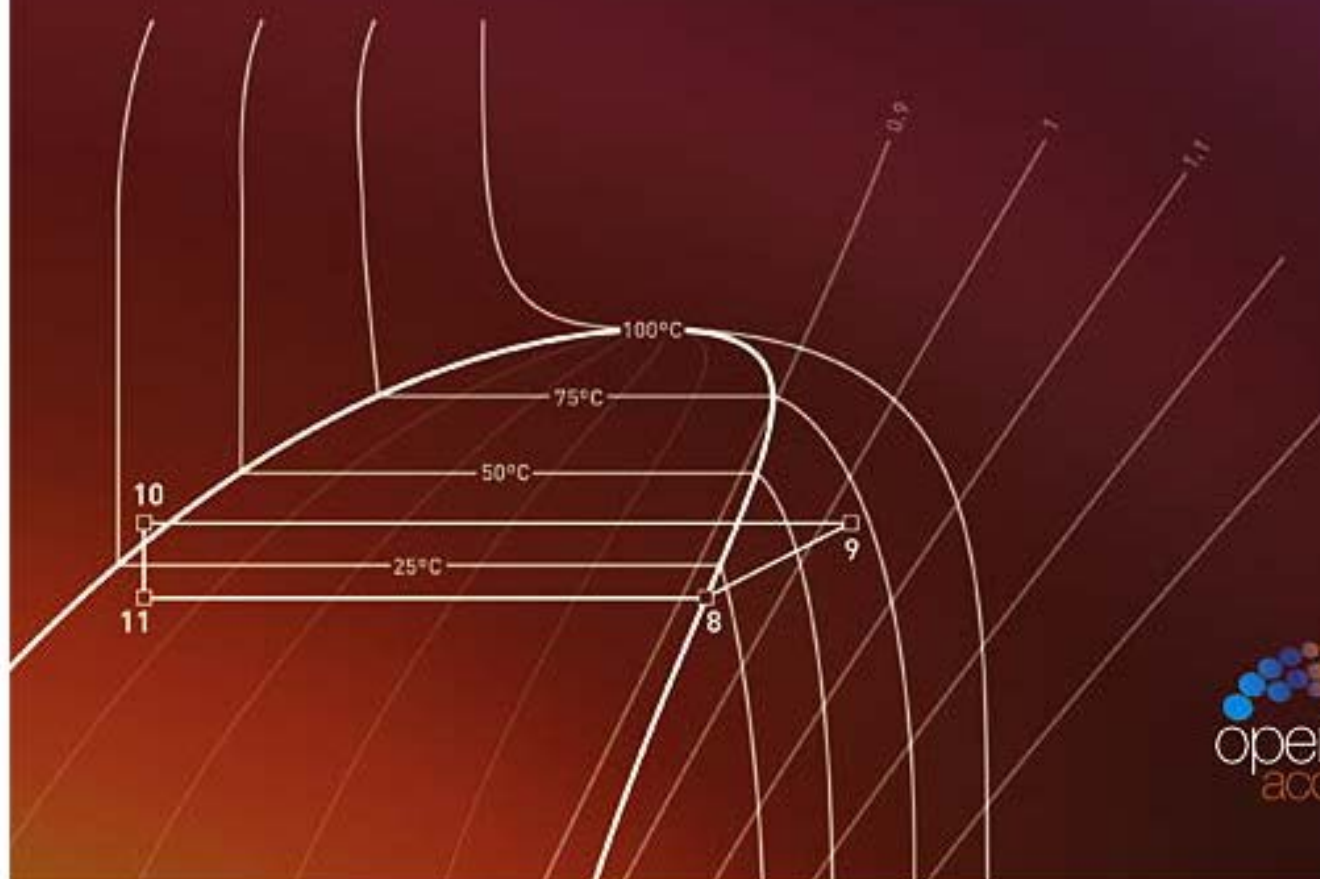




CASE STUDIES IN THERMAL ENGINEERING

EDITOR-IN-CHIEF: HUIHE QIU
HONG KONG UNIVERSITY OF SCIENCE AND TECHNOLOGY





Related Publications

Applied Thermal Engineering

Case Studies in Construction Materials (<https://www.elsevier.com/locate/inca/730455>)

Case Studies in Thermal Engineering - Editorial Board

Editor-in-Chief

H. Qiu (<https://www.journals.elsevier.com:443/case-studies-in-thermal-engineering/editorial-board/h-qiu>)

Hong Kong University of Science and Technology, Kowloon, Hong Kong, China

Email H. Qiu (<https://www.journals.elsevier.com:443/case-studies-in-thermal-engineering/editorial-board/h-qiu>)

Editorial Board Members

D. Attinger

Iowa State University, Ames, Iowa, USA

B. B. Feng

Xi'an Jiaotong University, Xi'an, Shaanxi, China

F. Hong

Shanghai Jiao Tong University, Shanghai, China

N. Huber

University of Applied Sciences, Weihenstephan-Triesdorf, Germany

J. F. Elmer

University of Florida, Gainesville, Florida, USA



SEARCH



MENU

Baden-Wuerttemberg Cooperative State University, Mosbach, Germany

(<https://www.elsevier.com>)

A. F. Miguel

Universidade de Évora, Évora, Portugal

D. A. Reay

David Reay & Associates, Whitley Bay, UK

A. Wang

National Taiwan University, Taipei, Taiwan

X. Wang

University of Science and Technology of China (USTC), Hefei, China

J. Xamán

National Center for Research and Technology Development (CENIDET), Cuernavaca, Morelos, Mexico

Case Studies in Thermal Engineering

Readers

View Articles

Volume/ Issue Alert

Personalized Recommendations

Authors (<http://www.elsevier.com/authors/home>)

Author Information Pack (<https://www.elsevier.com/journals/case-studies-in-thermal-engineering/2214-157X?generatepdf=true>)

Submit Your Paper

Track Your Paper

Early Career Resources (<http://www.elsevier.com/early-career-researchers/training-and-workshops>)

Rights and Permissions (<https://www.elsevier.com/about/policies/copyright/permissions>)

Support Center

Librarians (<https://www.elsevier.com/librarians>)

Abstracting/ Indexing (<http://www.elsevier.com/journals/case-studies-in-thermal-engineering/2214-157X/abstracting-indexing>)



ScienceDirect



Case Studies in Thermal Engineering

[OPEN ACCESS](#)

[Articles in press](#)

[Latest issue](#)

[All issues](#)

[About the journal](#) ↗

[Follow journal](#)

Volume 12

In progress (September 2018)

This issue is in progress but contains articles that are final and fully citable.

[< Previous vol/issue](#)

[Next vol/issue >](#)



Expand all article previews



Download PDFs



Export


- ☐ Short communication *Open access*
Some solar passive concepts in habitat through natural ventilation case study:
Dry climate in Algeria Ghardaia
M.K. Cherier, T. Benouaz, S.M.A. Bekkouche, M. Hamdani
Pages 1-7

 [Download PDF](#) [Article preview](#) 

- ☐ Short communication *Open access*
Studies on energy consumption of crude oil pipeline transportation process
based on the unavoidable exergy loss rate
Qinglin Cheng, Anbo Zheng, Lu Yang, Chenlin Pan, ... Yang Liu
Pages 8-15

 [Download PDF](#) [Article preview](#) 

- ☐ Short communication *Open access*
Carreau fluid flow in a thermally stratified medium with heat
generation/absorption effects
Khalil Ur Rehman, Ali Saleh Alshomrani, M.Y. Malik
Pages 16-25

 [Download PDF](#) [Article preview](#) 

- ☐ Short communication *Open access*
An integrated program of a stand-alone parabolic trough solar thermal power
plant: Code description and test
Sanan T. Mohammad, Hussain H. Al-Kayiem, Morteza K. Assadi, Osama. Sabir, Ayad K. Khelif
Pages 26-37

 [Download PDF](#) [Article preview](#) 

- ☐ Short communication *Open access*
On the conceptual design of the novel balanced rolling piston expander
Antonio Giuffrida, Gianluca Valenti, Davide Palamini, Luigi Solazzi
Pages 38-46

 [Download PDF](#) [Article preview](#) 

☐ Short communication [Open access](#)

Influence of mechanical smoke exhaust on smoke spread in underground tunnel

Hai jun Tao, Guoqing Zhu, Yu Xia, Yongchang Zhao

Pages 47-54

 [Download PDF](#) [Article preview](#) 

☐ Short communication [Open access](#)

Exhaust noise, performance and emission characteristics of spark ignition engine fuelled with pure gasoline and hydrous ethanol gasoline blends

Xiaokang Deng, Zhenbin Chen, Xiaochen Wang, Haisheng Zhen, Rongfu Xie

Pages 55-63

 [Download PDF](#) [Article preview](#) 

☐ Short communication [Open access](#)

Case study on thermal impact of novel corrosion inhibitor on mild steel

Hussein Jwad Habeeb, Hasan Mohammed Luaibi, Thamer Adnan Abdullah, Rifaat Mohammed

Dakhil, ... Ahmed A. Al-Amiery

Pages 64-68

 [Download PDF](#) [Article preview](#) 

☐ Short communication [Open access](#)

Experimental study on smoke temperature distribution under different power conditions in utility tunnel

Yong-chang Zhao, Guo-qing Zhu, Yun-ji Gao

Pages 69-76

 [Download PDF](#) [Article preview](#) 

☐ Short communication [Open access](#)

Experimental and theoretical research on the fire safety of a building insulation material via the ignition process study

Yufeng Huang, Yufeng Li

Pages 77-84



[Download PDF](#)

[Article preview](#)



Short communication *Open access*

Forecasting the heating and cooling load of residential buildings by using a learning algorithm “gradient descent”, Morocco

Alaoui Sosse Jihad, Mohamed Tahiri

Pages 85-93



[Download PDF](#)

[Article preview](#)



Short communication *Open access*

Combined heat loss analysis of trapezoidal shaped solar cooker cavity using computational approach

Jayashree Nayak, Mohit Agrawal, Saumyakanta Mishra, Sudhansu S. Sahoo, ... Antaryami Mishra

Pages 94-103



[Download PDF](#)

[Article preview](#)



Short communication *Open access*

Numerical thermodynamic model of alpha-type Stirling engine

Khaled M. Bataineh

Pages 104-116



[Download PDF](#)

[Article preview](#)



Short communication *Open access*

Numerical simulation of fluid solid coupling heat transfer in tunnel

Du Cuifeng, Bian Menglong

Pages 117-125



[Download PDF](#)

[Article preview](#)



Short communication *Open access*

Thermal and concentration aspects in Carreau viscosity model via wedge

Usman Ali, Khalil Ur Rehman, Ali Saleh Alshomrani, M.Y. Malik

Pages 126-133



[Download PDF](#)

[Article preview](#)



Short communication *Open access*

Experimental and numerical studies on ceiling maximum smoke temperature and longitudinal decay in a horseshoe shaped tunnel fire

Yunji Gao, Guoqing Zhu, Sinian Gu, Haijun Tao, Yongchang Zhao

Pages 134-142



[Download PDF](#)

[Article preview](#)



Short communication *Open access*

Heat release analysis and thermal efficiency of a single cylinder diesel dual fuel engine with gasoline port injection

Chondanai Vipavanich, Sathaporn Chuepeng, Sompol Skullong

Pages 143-148



[Download PDF](#)

[Article preview](#)



Short communication *Open access*

Mathematical modeling and simulation of a solar agricultural dryer with back-up biomass burner and thermal storage

Elieser Tarigan

Pages 149-165



[Download PDF](#)

[Article preview](#)



Short communication *Open access*

New advancement of high performance for a combined cycle power plant: Thermodynamic analysis

M.N. Khan, I. Tlili

Pages 166-175



[Download PDF](#)

[Article preview](#)



Short communication *Open access*

Nonlinear thermal radiation effect on magneto Casson nanofluid flow with Joule heating effect over an inclined porous stretching sheet

S.S. Ghadikolaei, Kh. Hosseinzadeh, D.D. Ganji, B. Jafari

Pages 176-187



[Download PDF](#)

[Article preview](#)



Short communication *Open access*

Effect of cooled EGR on modified light duty diesel engine for combustion, performance and emissions under high pressure split injection strategies

Gautam Edara, Y.V.V. Satyanarayana Murthy, Paleti Srinivas, Jayashri Nayar, Merigala Ramesh

Pages 188-202



[Download PDF](#)

[Article preview](#)



Short communication *Open access*

Thermo-physical aspects in tangent hyperbolic fluid flow regime: A short communication

Khalil Ur Rehman, Ali Saleh Alshomrani, M.Y. Malik, Iffat Zehra, Muhammad Naseer

Pages 203-212



[Download PDF](#)

[Article preview](#)



Short communication *Open access*

Heat transfer phenomena on waste heat recovery of combustion stack gas with deionized water in helical coiled heat exchanger

Rithy Kong, Thoranis Deethayat, Attakorn Asanakham, Tanongkiat Kiatsiriroat

Pages 213-222



[Download PDF](#)

[Article preview](#)



Short communication *Open access*

Experimental analysis of using beeswax as phase change materials for limiting temperature rise in building integrated photovoltaics

Razali Thaib, Samsul Rizal, Hamdani, T.M.I. Mahlia, Nugroho Agung Pambudi

Pages 223-227



[Download PDF](#)

[Article preview](#)

☐ Short communication *Open access*

A numerical investigation on ethylene glycol-titanium dioxide nanofluid convective flow over a stretching sheet in presence of heat generation/absorption

Kh. Hosseinzadeh, F. Afsharpanah, S. Zamani, M. Gholinia, D.D. Ganji
Pages 228-236

 [Download PDF](#) [Article preview](#) 

☐ Short communication *Open access*

The effect of multi-longitudinal vortex generation on turbulent convective heat transfer within alternating elliptical axis tubes with various alternative angles

Hasan Najafi Khaboshan, Hamid Reza Nazif
Pages 237-247

 [Download PDF](#) [Article preview](#) 

☐ Short communication *Open access*

Determination of effective moisture diffusivity and thermodynamic properties variation of regional wastes under different atmospheres

Fernandez Anabel, Román Celia, Mazza Germán, Rodriguez Rosa
Pages 248-257

 [Download PDF](#) [Article preview](#) 

☐ Short communication *Open access*

Performance evaluation and parametric studies on variable nozzle ejector using R134A

B. Elhub, Sohif Mat, K. Sopian, A.M. Elbreki, ... A.A. Ammar
Pages 258-270

 [Download PDF](#) [Article preview](#) 

☐ Short communication *Open access*

Thermal analysis in Stokes' second problem of nanofluid: Applications in thermal engineering

Ilyas Khan, Kashif Ali Abro, M.N. Mirbhar, I. Tlili

Pages 271-275



[Download PDF](#)

[Article preview](#)



Short communication *Open access*

Detection of ammonia gas by Knudsen thermal force in micro gas actuator

Ahmadreza Mahyari, M. Barzegar Gerdroodbary, M. Mosavat, D.D. Ganji

Pages 276-284



[Download PDF](#)

[Article preview](#)



Short communication *Open access*

Use of parabolic troughs in HVAC applications – Design calculations and analysis

Khaled Chahine, Rabih Murr, Mohamad Ramadan, Hicham El Hage, Mahmoud Khaled

Pages 285-291



[Download PDF](#)

[Article preview](#)



Short communication *Open access*

Entropy generation in MHD mixed convection stagnation-point flow in the presence of joule and frictional heating

M.I. Afridi, M. Qasim, Ilyas Khan, I. Tlili

Pages 292-300



[Download PDF](#)

[Article preview](#)



Short communication *Open access*

Influence of thermal contact on heat transfer from glowing firebrands

Alok Warey

Pages 301-311



[Download PDF](#)

[Article preview](#)



Short communication *Open access*

Magnetically stirring enhanced thermal performance of phase change material

Dao-Yu Sun, Si-Xin Yan, Zhi-Zhu He

Pages 312-318

 [Download PDF](#) [Article preview](#) 

☐ Short communication [Open access](#)

Micropolar nanofluid flow and heat transfer between penetrable walls in the presence of thermal radiation and magnetic field

M. Alizadeh, A.S. Dogonchi, D.D. Ganji

Pages 319-332

 [Download PDF](#) [Article preview](#) 

☐ Short communication [Open access](#)

Lifted flame property and interchangeability of natural gas on partially premixed gas burners

Zhiguang Chen, Chaokui Qin, Pengfei Duan

Pages 333-339

 [Download PDF](#) [Article preview](#) 

☐ Short communication [Open access](#)

Magneto-Marangoni nano-boundary layer flow of water and ethylene glycol based γ Al_2O_3 nanofluids with non-linear thermal radiation effects

N. Vishnu Ganesh, Ali J. Chamkha, Qasem M. Al-Mdallal, P.K. Kameswaran

Pages 340-348

 [Download PDF](#) [Article preview](#) 

☐ Short communication [Open access](#)

Thermal characteristic research of associated power devices based on three-level inverters and power-loss calculation

Shi-Zhou Xu, Chun-Jie Wang, Fang-Li Lin, Xiang-Yu Zhu, Xue Xia

Pages 349-357

 [Download PDF](#) [Article preview](#) 

☐ Short communication [Open access](#)

Effect on TEG performance for waste heat recovery of automobiles using MgO and ZnO nanofluid coolants

Dhruv Raj Karana, Rashmi Rekha Sahoo

Pages 358-364



[Download PDF](#)

[Article preview](#)



Short communication *Open access*

Experimental study on upward flame spread characteristics of external thermal insulation material under the influence of porosity

Qing xuan Meng, Guo qing Zhu, Miao miao Yu, Zhen huan Liang

Pages 365-373



[Download PDF](#)

[Article preview](#)



Short communication *Open access*

Case study of MHD blood flow in a porous medium with CNTS and thermal analysis

Asma Khalid, Ilyas Khan, Arshad Khan, Sharidan Shafie, I. Tlili

Pages 374-380



[Download PDF](#)

[Article preview](#)



Short communication *Open access*

Hybrid thermal model of a synchronous reluctance machine

Payam Shams Ghahfarokhi, Ants Kallaste, Anouar Belahcen, Toomas Vaimann, Anton Rassölkin

Pages 381-389



[Download PDF](#)

[Article preview](#)



Short communication *Open access*

CFD-Based research on control strategy of the opening of Active Grille Shutter on automobile

JiaCheng Li, YaDong Deng, YiPing Wang, Chuqi Su, Xun Liu

Pages 390-395



[Download PDF](#)

[Article preview](#)



Short communication *Open access*

The energy and economic target optimization of a naphtha production unit by

implementing energy pinch technology

Ali Manizadeh, Ashkan Entezari, Rouhollah Ahmadi

Pages 396-404



[Download PDF](#)

[Article preview](#)



Short communication *Open access*

Numerical study on the effect of operating nanofluids of photovoltaic thermal system (PV/T) on the convective heat transfer

Ali H.A. Al-Waeli, Miqdam T. Chaichan, Hussein A. Kazem, K. Sopian, Javad Safaei

Pages 405-413



[Download PDF](#)

[Article preview](#)



Short communication *Open access*

Optical efficiency measurement of solar receiver tubes: A testbed and case studies

Rafael López-Martín, Loreto Valenzuela

Pages 414-422



[Download PDF](#)

[Article preview](#)



Short communication *Open access*

Some particular design considerations for optimum utilization of under floor heating systems

S. Oubenmoh, A. Allouhi, A. Ait Mssad, R. Saadani, ... M. Bentaleb

Pages 423-432



[Download PDF](#)

[Article preview](#)



Short communication *Open access*

Effect of the particle size of pulverized olive cake on combustion parameters in Stirling engine in Morocco

N. Rassai, N. Boutammachte, H. El hassani, A. Al Mers, ... A. Bekraoui

Pages 433-444



[Download PDF](#)

[Article preview](#)

☐ Short communication *Open access*

Numerical evaluation of the effects of fire on steel connections; Part 1: Simulation techniques

Rohola Rahnavard, Robert J. Thomas

Pages 445-453



[Download PDF](#)

[Article preview](#)

☐ Short communication *Open access*

Effect of interfacial thermal resistance and nanolayer on estimates of effective thermal conductivity of nanofluids

Ali Khodayari, Matteo Fasano, Masoud Bozorg Bigdeli, Shahin Mohammadnejad, ... Pietro Asinari

Pages 454-461



[Download PDF](#)

[Article preview](#)

☐ Short communication *Open access*

Thermal aspects of Carreau fluid around a wedge

Usman Ali, Khalil Ur Rehman, M.Y. Malik, Iffat Zehra

Pages 462-469



[Download PDF](#)

[Article preview](#)

☐ Short communication *Open access*

Numerical simulation for the heat transfer behavior of oil pipeline during the shutdown and restart process

Lixin Wei, Qimeng Lei, Jian Zhao, Hang Dong, Lin Yang

Pages 470-483



[Download PDF](#)

[Article preview](#)

☐ Short communication *Open access*

Optimisation of tilted angles of a photovoltaic cell to determine the maximum generated electric power: A case study of some Iraqi cities

Akeel M. Ali Morad, Ali K. Shaker Al-Sayyab, Mohammed A. Abdulwahid

Pages 484-488

 [Download PDF](#) [Article preview](#) 

☐ Short communication *Open access*

Fabrication and testing of hybrid solar-biomass dryer for drying fish

Hamdani, T.A. Rizal, Zulfri Muhammad

Pages 489-496

 [Download PDF](#) [Article preview](#) 

☐ Short communication *Open access*

Numerical investigation of heat transfers in the water jacket of heavy duty diesel engine by considering boiling phenomenon

M. Gholinia, M. Pourfallah, H.R. Chamani

Pages 497-509

 [Download PDF](#) [Article preview](#) 

☐ Short communication *Open access*

Actual validation of energy simulation and investigation of energy management strategies (Case Study: An office building in Semnan, Iran)

Afshin Fathalian, Hadi Kargarsharifabad

Pages 510-516

 [Download PDF](#) [Article preview](#) 

☐ Short communication *Open access*

Studies of the unavoidable exergy loss rate and analysis of influence parameters for pipeline transportation process

Qinglin Cheng, Anbo Zheng, Lu Yang, Hao Wu, ... Yang Liu

Pages 517-527

 [Download PDF](#) [Article preview](#) 

☐ Short communication *Open access*

Validated mathematical models of a solar water heater system with thermosyphon evacuated tube collectors

C. Wannagosit, P. Sakulchangsatjatai, N. Kammuang-lue, P. Terdtoon

Pages 528-536



[Download PDF](#)

[Article preview](#)



Short communication *Open access*

An investigation of dynamic behavior of the cylindrical shells under thermal effect

Adawiya Ali Hamzah, Hussein K. Jobair, Oday I. Abdullah, Emad Talib Hashim, Laith A. Sabri
Pages 537-545



[Download PDF](#)

[Article preview](#)



Short communication *Open access*

Pyrolysis behavior and kinetics of corn residue pellets and eucalyptus wood chips in a macro thermogravimetric analyzer

Thossaporn Onsree, Nakorn Tippayawong, Anqing Zheng, Haibin Li
Pages 546-556



[Download PDF](#)

[Article preview](#)



Short communication *Open access*

Assessment of heat transfer and fluid flow characteristics within finned flat tube

Maki H. Zaidan, Aadel A.R. Alkumait, Thamir K. Ibrahim
Pages 557-562



[Download PDF](#)

[Article preview](#)



Short communication *Open access*

Performance analysis of shell and tube heat exchanger: Parametric study

Ammar Ali Abd, Mohammed Qasim Kareem, Samah Zaki Naji
Pages 563-568



[Download PDF](#)

[Article preview](#)



Short communication *Open access*

Analysis on the influence of the smoke block board on the entrainment phenomena near a mechanical exhaust vent

Zhisheng Xu, Hongguang Chen, Lu He, Jiaming Zhao, ... Baochao Xie

Pages 569-577



[Download PDF](#)

[Article preview](#)



Short communication *Open access*

Hybrid semi analytical method for geothermal U shaped heat exchanger

P. Jalili, D.D. Ganji, S.S. Nourazar

Pages 578-586



[Download PDF](#)

[Article preview](#)



Short communication *Open access*

Numerical investigation of V-groove air-collector performance with changing cover in Bangi, Malaysia

Idris Zulkifle, Ali H.A. Alwaeli, Mohd Hafidz Ruslan, Zahari Ibarahim, ... Kamaruzzaman Sopian

Pages 587-599



[Download PDF](#)

[Article preview](#)



Short communication *Open access*

Heat transfer enhancement and pressure drop of Fe_3O_4 -water nanofluid in a double tube counter flow heat exchanger with internal longitudinal fins

Mohammad Sikindar Baba, A.V. Sita Rama Raju, M. Bhagvanth Rao

Pages 600-607



[Download PDF](#)

[Article preview](#)



Short communication *Open access*

Numerical optimization on thermal performance characteristics of interior walls based on air-conditioning intermittent running

Xi Meng, Wentao Hu, Ying Cao, Yisheng Huang, ... Yanna Gao

Pages 608-619



[Download PDF](#)

[Article preview](#)



Short communication *Open access*

Thermal and hydraulic characteristics of turbulent nanofluids flow in

trapezoidal-corrugated channel: Symmetry and zigzag shaped

Raheem K. Ajeel, W.S-I. W. Salim, Khalid Hasnan

Pages 620-635



[Download PDF](#)

[Article preview](#)



Short communication *Open access*

Numerical investigation of heat transfer from multi-bulges pins

Amr Owes Elsayed

Pages 636-643



[Download PDF](#)

[Article preview](#)



Short communication *Open access*

Bree's diagram of a functionally graded thick-walled cylinder under thermo-mechanical loading considering nonlinear kinematic hardening

Mohsen Damadam, Reza Moheimani, Hamid Dalir

Pages 644-654



[Download PDF](#)

[Article preview](#)



Short communication *Open access*

Flow characteristics of two dimensional classical and pulsating jet in crossflow at low Reynolds number

Jianlong Chang, Xudong Shao, Jiangman Li

Pages 655-665



[Download PDF](#)

[Article preview](#)



Short communication *Open access*

Case study on solar water heating for flat plate collector

Walaa Mousa Hashim, Ali Talib Shomran, Hasan Ali Jurmut, Tayser Sumer Gaaz, ... Ahmed A. Al-Amiery

Pages 666-671



[Download PDF](#)

[Article preview](#)



Short communication *Open access*

Preliminary assessment of a solar absorption air conditioning pilot plant

P. Soto, L.A. Domínguez-Inzunza, W. Rivera

Pages 672-676



[Download PDF](#)

[Article preview](#)



Short communication *Open access*

Drying behaviour of lemon balm leaves in an indirect double-pass packed bed forced convection solar dryer system

Shahrbanou Shamekhi-Amiri, Tahereh B. Gorji, Mofid Gorji-Bandpy, Mohammad Jahanshahi

Pages 677-686



[Download PDF](#)

[Article preview](#)



Short communication *Open access*

The effect of solar radiation on the energy consumption of refrigerated container

Muhammad Arif Budiyanto, Takeshi Shinoda

Pages 687-695



[Download PDF](#)

[Article preview](#)



Short communication *Open access*

Optimization of area ratio and thrust in suddenly expanded flow at supersonic Mach numbers

Khizar Ahmed Pathan, P.S. Dabeer, Sher Afghan Khan

Pages 696-700



[Download PDF](#)

[Article preview](#)



Short communication *Open access*

Average view factors for extended surfaces with fractal perforations

David Calamas, Daniel Dannelley

Pages 701-710



[Download PDF](#)

[Article preview](#)



Short communication *Open access*

Extraction of bio-oil during pyrolysis of locally sourced palm kernel shells:

Effect of process parameters

J.O. Ogunkanmi, D.M. Kulla, N.O. Omisanya, M. Sumaila, ... D. Dodoo-Arhin

Pages 711-716



[Download PDF](#)

[Article preview](#)



Short communication *Open access*

Influence of the oblique fin arrangement on the fluid flow and thermal performance of liquid cold plate

Nur Irmawati Om, Rozli Zulkifli, P. Gunnasegaran

Pages 717-727



[Download PDF](#)

[Article preview](#)



Short communication *Open access*

Control of electric power generation of thermal power plant in TamilNadu

M.S. Murshitha Shajahan, V. Aparna, D. Najumnissa Jamal, M.K.A. Ahamed Khan

Pages 728-735



[Download PDF](#)

[Article preview](#)



Short communication *Open access*

Cycle improvement and hydrogen steam superheating at Mutnovsky geothermal power plant

D.O. Dunikov

Pages 736-741



[Download PDF](#)

[Article preview](#)

ISSN: 2214-157X

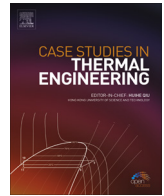
Copyright © 2018 Elsevier Ltd. All rights reserved



We use cookies to help provide and enhance our service and tailor content and ads. By continuing you agree to the [use of cookies](#).

Copyright © 2018 Elsevier B.V. or its licensors or contributors. ScienceDirect® is a registered trademark of Elsevier B.V.





Mathematical modeling and simulation of a solar agricultural dryer with back-up biomass burner and thermal storage

Elieser Tarigan

Center for Renewable Energy and Department of Electrical Engineering, Faculty of Engineering, University of Surabaya, Jl. Raya Kalirungkut, Surabaya 60292, Indonesia

ARTICLE INFO

Keywords:

Solar dryer
Solar drying
Mathematical modeling
CFD
Simulation

ABSTRACT

Solar drying is a cost-effective and environmentally friendly method for drying agricultural products. To design a proper solar dryer for specific products, thermodynamic relations for the dryer system need to be considered. Numerical simulations are commonly used for the design and operational control of dryers. This study presents the mathematical modeling and simulation of a solar agricultural dryer with back-up biomass burner and thermal storage. Thermodynamic and numerical simulations of the solar collector and drying chamber are performed, while back-up heater (biomass burner) operation is simulated with a computational fluid dynamics (CFD) simulation. For the solar collector, it was found that the presence of a glass cover significantly increases the temperature of the collector; however, increasing the number of glass covers from one to two does not significantly affect the temperature. Variation in thickness of the back insulation has negligible effects, especially for thicknesses over 3 cm. The results show that there is a small difference in temperature between the bottom three trays, while the temperature on the top tray is significantly higher. The CFD simulation showed that the average drying air temperature in the drying chamber was 56 °C, which is suitable for the drying of agricultural products.

1. Introduction

Drying is an effective method of food or agricultural product preservation for long periods. In general, farmers face problems in having their products dried fast, efficiently, economically, and in a correct environmental fashion. Sun drying on the ground is currently the most used method. Most farmers, especially in developing countries, cannot afford to import expensive drying equipment, which is either electrically or diesel-engine driven. This causes additional financial burdens of maintenance, fuel, electricity, and other running expenses in addition to environmental problems. Solar drying has been well-known as a cost-effective drying method; it is widely used worldwide and is environmentally friendly.

Solar dryer systems can be classified into direct and indirect dryers. For direct dryers, solar radiation is absorbed directly by the product to be dried, while indirect dryers use solar radiation to heat the air, which then flows through the space containing the product [1]. Indirect solar dryers employ a separate solar collector that absorbs solar radiation, converts it into thermal energy that in turn heats the flowing air, and then supplies the heated air to a chamber. A combination of direct and indirect methods is called a mixed-type dryer [2].

Based on the auxiliary energy used to operate the system, dryers are classified into active and passive dryers. Active dryers employ an external means such as fans or blowers to move the heated air from the solar collector to the drying bed, while passive dryers use

E-mail address: elieser@staff.ubaya.ac.id.

<https://doi.org/10.1016/j.csite.2018.04.012>

Received 20 February 2018; Received in revised form 28 March 2018; Accepted 11 April 2018

Available online 12 April 2018

2214-157X/ © 2018 The Author. Published by Elsevier Ltd. This is an open access article under the CC BY license (<http://creativecommons.org/licenses/by/4.0/>).

Nomenclature			
A	surface area of solar collector (m^2)	q	total heat gain (W m^{-2})
A_p	specific surface area of products ($\text{m}^2 \text{ m}^{-3}$)	Re	Reynolds number
A_s	surface area of tray (m^2)	T	temperature ($^{\circ}\text{C}$)
A_w	surface area of the wall of chamber (m^2)	T_a	ambient temperature ($^{\circ}\text{C}$)
b	width of the collector (m)	$T_{b,m}$	mean temperature of back plate ($^{\circ}\text{C}$)
C_a	specific heat of dry air ($\text{J kg}^{-1} \text{ K}^{-1}$)	$T_{b,x}$	temperature of back plate ($^{\circ}\text{C}$)
C_p	specific heat of air ($\text{J kg}^{-1} \text{ K}^{-1}$)	$T_{f,m}$	mean temperature of air in the collector ($^{\circ}\text{C}$)
C_v	specific heat of water vapor ($\text{J kg}^{-1} \text{ K}^{-1}$)	$T_{f,x}$	temperature of air in the collector ($^{\circ}\text{C}$)
d	depth of products in the tray (m)	$T_{p,m}$	mean temperature of absorber plate ($^{\circ}\text{C}$)
g_i	the gravitational acceleration vector (m/s^2)	$T_{p,x}$	temperature of absorber plate ($^{\circ}\text{C}$)
h_{a-b}	convective heat transfer coefficient between air and bottom ($\text{W m}^{-2} \text{ K}^{-1}$)	T_{sky}	sky temperature ($^{\circ}\text{C}$)
h_{a-p}	convective heat transfer coefficient between air and tray ($\text{W m}^{-2} \text{ K}^{-1}$)	\bar{T}	the mean temperature
h_{a-w}	convective heat transfer coefficient between air and chamber wall ($\text{W m}^{-2} \text{ K}^{-1}$)	\bar{T}'	the temperature fluctuation
h_b	convective coefficient heat transfer from back plate to the flowing air ($\text{W m}^{-2} \text{ K}^{-1}$)	T_{ref}	the reference temperature
h_p	convective coefficient heat transfer from absorber to the flowing air ($\text{W m}^{-2} \text{ K}^{-1}$)	T_w	temperature of the wall of chamber (K)
h_r	radiative coefficient heat transfer between absorber and back plate ($\text{W m}^{-2} \text{ K}^{-1}$)	\bar{u}	the mean velocity components
i	order number of trays, counted from bottom ($i = 1, 2, 3, \dots$)	\bar{u}'	the velocity fluctuation
I	solar radiation intensity (W m^{-2})	U_b	coefficient of total heat loss from bottom surface ($\text{W m}^{-2} \text{ K}^{-1}$)
k	turbulent kinetic energy	U_p	total heat loss from top surface ($\text{W m}^{-2} \text{ K}^{-1}$)
k_w	conductive heat transfer of wall ($\text{W m}^{-2} \text{ K}^{-1}$)	w	humidity ratio of air (kg kg^{-1})
L_e	latent heat of evaporation (kJ kg^{-1})	<i>Greek</i>	
M	moisture content of products (decimal, d.b.)	β	the thermal expansion coefficient
\dot{m}	air mass flow rate (kg s^{-1})	ρ	the density
m_a	air mass flow rate (kg s^{-1})	δ_{ij}	Kronecker delta
N	number of glass covers	ε	emissivity
Nu	Nusselt number	ε_g	emissivity of the glass cover
\bar{P}	Pressure (Pa)	ε_p	emissivity of the absorber plate
		μ	viscosity
		μ_t	the turbulent
		ρ_p	density of products
		σ	Stefan-Boltzmann constant
		σ_H	turbulent-Prandtl number
		Γ_t	turbulent scalar diffusivity

only the natural movement of heated air. The drying of agricultural products involves two fundamental processes: evaporation of moisture from the surface, and migration of moisture from the interior of a substance to the surface.

To design a proper solar dryer for specific products, thermodynamic relations for the dryer system need to be considered. Several previous works involving numerical simulations have been reported. Bala and Woods [3] presented a technique for the optimization of passive solar dryers. A physical simulation was combined with a cost prediction and experimental techniques, which found the constrained minimum of the total cost per unit of moisture removal. The result of a sensitivity analysis indicated that the design geometry is insensitive to material or fixed costs. Slimani et al. [4] studied and modeled the energy performance of a hybrid photovoltaic/thermal solar collector, a configuration suitable for an indirect solar dryer. The results noted the importance of certain parameters and operating conditions on the performance of the hybrid collector.

Duran and Condori [5] simulated a passive solar dryer for charqui production using temperature and pressure networks. The results indicated that the drying time can be reduced by improvements to the constructive aspects of the dryer, the thermal isolation, and the air flow that passes up and down the trays. Simate [6] presented a comparison of optimized mixed-mode and indirect-mode passive solar dryers for maize. The optimization yielded a shorter collector length for the mixed-mode dryer than for the indirect-mode dryer. Khadraoui et al. [7] studied the thermal behavior of an indirect solar dryer with the nocturnal usage of a solar air collector with phase change material (PCM). It was reported that an indirect solar dryer (ISD) with paraffin wax as an energy storage material is an effective design to yield more favorable conditions for the drying process as compared to an ISD without energy storage.

Daghigh and Abdellah [8] presented an experimental study of a heat pipe evacuated tube solar dryer with a heat recovery system. The most accurate equation for expressing the effectiveness of this dryer was obtained by using a regression analysis. Bennamoun and Belhamri [9] studied a thermal performance analysis of an indirect-type active cabinet solar dryer. Shrinkage of the products was also taken into account. The results showed that drying was affected by the collector surface, the air temperature, and the product characteristics. Bahnasawy and Shenana [10] developed a mathematical model of direct sun and solar drying of some fermented dairy products (kishk). The model was able to predict the drying temperatures across a wide range of relative humidity values. The

model also had the capability to predict the moisture loss from the product in wide ranges of relative humidity values, temperatures, and air velocities. There are many more investigations of solar drying systems devoted to theoretical simulations [11–17].

In this study, we focus on a design method for an appropriate solar dryer with back-up biomass heater by using mathematical modeling and simulations. The designed dryer is intended to be used for drying agricultural products (e.g., candle nuts, coffee, chili, ground nuts, soybeans, and mung beans) that have high potential for using solar dryers in Southeast Asia, especially in Indonesia and Thailand [18,19]. Thermodynamic simulations of the solar collector and drying chamber are performed. In addition, a computational fluid dynamics (CFD) simulation of the air temperature and velocity inside the drying chamber in back-up biomass energy mode is performed. The key features of the solar dryer in this study are the biomass burner and back-up heating system which employing the bricks as a low cost heat storage, combination of direct and indirect type (so called mixed mode), and employing the jacket and gap enclosing the drying chamber as a hot gas passage. The features are expected to improve the viability of the solar dryer. The results from this study can be used to design and/or optimize an appropriate solar dryer with back-up biomass heater for drying agricultural products mentioned above.

2. Dryer design and components

2.1. Design considerations

Several considerations are taken into account for the design, including the types of product to be dried, the product's physical drying characteristics, the capacity and size of the dryer, and the materials for construction. The dryer designed in this study is intended for use to dry several products identified in previous works [18,19], as previously mentioned in Section 1.

The drying characteristics are some of the most important parameters for designing a solar dryer. A solar dryer designed for a certain kind of product may not be suitable for another product. Hence, the development of solar drying technology for the agricultural field should begin with studying the drying characteristics of specific agricultural products. After the information on the drying characteristics of products (such as drying rate, equilibrium moisture content, and other essential parameters) are known, mathematical modeling and computer simulations can be used to predict an appropriate and economical design for a solar dryer. In this study, the results of studies on candle-nut drying characteristics, as described in [19], will be used in the simulations.

The dryer is intended for use by an individual (household) farmer; hence, its capacity and size are designed accordingly. Results from a field survey indicated that individual farmers (in this case, located in Indonesia) need to dry about 100–200 kg of candle nuts per day on average. The bulk density of fresh candle nuts is about 600 kg/m^3 . By using candle nuts as the main product to determine the dryer capacity, and assuming that the drying process occurs in a thin layer with the thickness of the bed product at 3 cm, then the area of the tray should be about 11 m^2 . It was also estimated that the capacity of the dryer needed for other products was approximately the same.

The solar collector system is made of a zinc metal plate painted black, with a single-layer typical glass cover. The backside is insulated with mineral wool. The biomass burner and thermal storage system are made of construction bricks. The drying chamber is framed with metal bars and walled with zinc plates (internal) and an insulated wall with mineral wool (external).

2.2. Dryer construction

The main parts of the dryer are the solar collector, the biomass burner, and the drying chamber. The solar dryer design is a mixed-

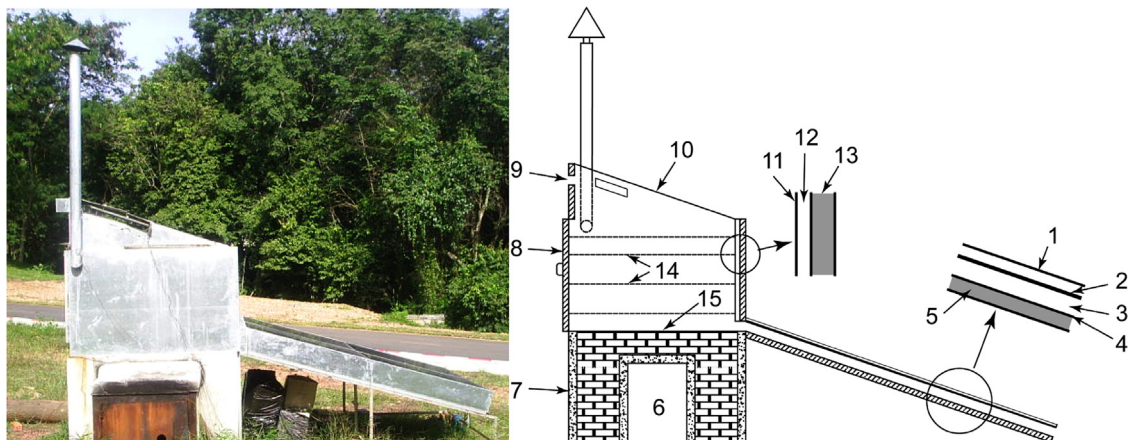


Fig. 1. Photograph and side-view diagram of dryer. Numeric description: 1. Glass cover for solar collector, 2. Absorber plate, 3. Space for inlet air, 4. Bottom plate for solar collector, 5. Insulation, 6. Space for biomass burning, 7. Thermal storage, 8. Loading door with insulation, 9. Ventilation slots, 10. Glass cover for drying chamber, 11. Internal wall, 12. Gap for hot gas passage, 13. External wall with insulation, 14. Perforated trays, 15. Bottom plate for drying chamber.

mode passive cabinet type, adopted from our previous work [2]. A photograph and schematic diagram of the dryer are shown in Fig. 1.

2.2.1. Solar collector system

The 2.75-by-1.75-m solar collector system consists of an absorber, a single-layer glass cover, a back plate, and insulation. The absorber is made from a 0.5-mm-thick black-painted metal (zinc) plate. A single layer of a typical glass cover with a thickness of 5 mm is placed on top of the collector. The backside and edges of the collector are insulated with 3-cm-thick mineral wool to reduce heat loss. The air-sealed gap between the absorber and the glass cover is 50 mm wide, and between the absorber and the back plate is a space of 100 mm. The solar collector system has a tilt of 19° from the horizontal level and faces south. This maximizes the solar radiation reception throughout the year and prevents rainwater from stagnating in the collector.

2.2.2. Back-up heater-biomass burner

A biomass burner with overall dimensions of $1.75\text{ m} \times 0.9\text{ m} \times 1.5\text{ m}$ is constructed along with the back-up heating system of the solar dryer. The wall is made from concrete, and the thermal storage space is filled with bricks. In the biomass burner, the free space for biomass feeding is $0.75\text{ m} \times 0.5\text{ m} \times 1\text{ m}$. The space includes a $0.75\text{ m} \times 0.5\text{ m} \times 0.25\text{ m}$ extruded wall at the outside of the burner. There is a door of $0.75\text{ m} \times 0.5\text{ m}$ at the front side of the extruded wall. A rectangular slit of $0.1\text{ m} \times 0.4\text{ m}$ at the lower edge of the door acts as a fresh air inlet to the burner during burning. The bricks used for heat storage are arranged in a manner in which the exhaust gas and smoke from combustion pass between all stones before venting out to the atmosphere, in order to maximize the capture of heat from the exhausted gas.

2.2.3. Drying chamber

The drying chamber is installed above the biomass burner and the thermal storage. It consists of a 19° -tilted single-layer glass cover on the top of the chamber with its trays. The trays/rack consist of four shelves with two trays on each shelf. The effective dimensions of a single tray are $1.45\text{ m} \times 0.82\text{ m}$. The trays are made of a perforated zinc plate and are supported with metal bars. The distance between trays is 150 mm. The bottom plate of the drying chamber is placed directly on top of the thermal storage unit. The external walls consist of 50-mm-thick insulation (mineral wool) covered with a zinc sheet. The internal walls are made of zinc sheet. A 40-mm free space between the internal and external walls forms a “jacket” around three sides of the chamber, which allows the exhausted gas that passes through the thermal storage to flow, before it is released to the ambient area through the chimney. This keeps the drying chamber warm. The chimney is attached to the upper edge on the right side of the jacket.

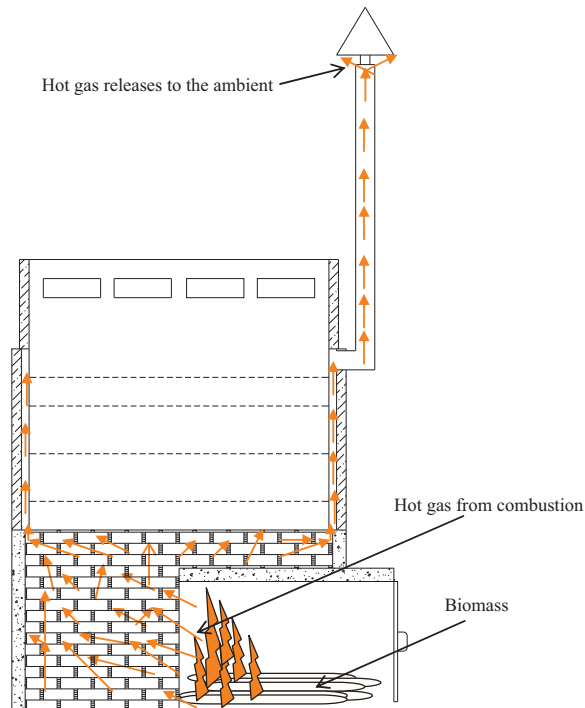


Fig. 2. Schematic diagram operation of dryer during the biomass back-up heater mode.

2.3. Dryer operation

The dryer can be operated in three different modes, i.e., (i) solar energy mode, (ii) back-up heater mode, and (iii) combination of solar energy and back-up heater mode. The first mode is applied during day time when solar radiation is high enough as the heat source produced through solar collector. This mode is commonly applied for a solar dryer in general. The second mode can be used at night and/or during low solar radiation, while combination of solar energy and back-up heater (third mode) can be applied used during daytime, e.g. for continuously drying during uncertain weather condition.

Schematic diagram operation of dryer during the biomass back-up heater mode is illustrated in Fig. 2. The hot gas passes between the stored bricks, flows through the jacket, and finally arrives at the ambient. When the combustion in the burner was over, the stored heat in the bricks might be started to contribute to the drying air. In this case, for the next day, the source of heat would be from both solar energy and stored heat in the brick (combination). It means that biomass burner and heat storage facility would improve the viability of solar dryer.

3. Prediction through modeling

Numerical simulations are commonly used for the design and operational control of dryers. Various simulation models for solar drying processes are found in the literature [3–6,9,10,15]. They differ mainly in the assumptions made and strategies employed to solve the model equation. A simplified mathematical model for the solar dryer was developed to analyze various designs in this study. The set of mathematical equations was solved by numerical simulation. In addition, a CFD simulation using FloVent was applied to predict the temperature distribution and air flow pattern in the drying chamber, especially during back-up heater operation.

3.1. Mathematical modeling

3.1.1. Thermal analysis of the solar collector system

The thermodynamic equation used for the solar collector was adopted from Ref. [22,23]. In developing the equations, the following assumptions were made:

- Temperatures were assumed to be uniform across the width of the collector, and the sides of the collector were assumed to be well insulated.
- The temperature gradients through the thicknesses of the plates were neglected.
- The effect of fouling on the plate was assumed to be negligible.
- The system was in a steady state.
- The temperature of the air flowing through the collector was assumed to be uniform over the entire depth of the flow channel.

The terms for each notation in Eqs. (1)–(48) are described in the nomenclature list.

Considering the surface area of the solar collector (Fig. 1), and using the above assumptions, the energy balance can be written as

$$I = q + U_p(T_{p,x} - T_a) + U_b(T_{b,x} - T_a) \quad (1)$$

The heat balance on the air stream can be written as

$$q = h_p(T_{p,x} - T_{f,x}) + h_b(T_{b,x} - T_{f,x}) \quad (2)$$

The heat balance on the bottom plate gives

$$h_r(T_{p,x} - T_{b,x}) = h_b(T_{b,x} - T_{f,x}) + U_b(T_{b,x} - T_a) \quad (3)$$

Solving Eqs. (1)–(3) gives:

$$T_{p,x} = T_a + \frac{S}{U_L''} - \frac{\Delta q}{U_L} \quad (4)$$

$$T_{f,x} = T_a + \frac{S}{U_L} - \frac{\Delta q}{F'U_L} \quad (5)$$

$$T_{b,x} = T_a + \frac{S}{U_L''} - \frac{\Delta q}{U_L'} \quad (6)$$

where

$$U_L = U_p + U_b \left(\frac{h_r(h_p + h_b) + h_b(U_p + h_p)}{h_r(h_p + h_b) + h_p(U_b + h_b)} \right) \quad (7)$$

$$U'_L = U_p + U_b \left(\frac{h_r(h_p + h_b) + h_b h_p}{h_r(h_p + h_b) + h_p(U_b + h_b) + h_p U_b} \right) \quad (8)$$

$$U''_L = U_p + U_b \left(\frac{h_r(h_p + h_b) + U_p(h_p + h_b) + h_b h_p}{h_r(h_p + h_b) + h_p U_b} \right) \quad (9)$$

$$U'''_L = U_p + U_b \left(\frac{h_r(h_p + h_b) + U_p(h_p + h_b) + h_b h_p - \frac{U_p^2}{U_b} h_b}{h_r(h_p + h_b) + h_p h_b + U_p h_b} \right) \quad (10)$$

$$F' = \frac{1}{1 + \left(\frac{h_r(U_p + U_b) + U_p(h_p + U_b)}{h_r(h_p + h_b) + h_p(U_b + h_b)} \right)} \quad (11)$$

The notations of U_L , U'_L , U''_L , and U'''_L represent the groupings of the heat transfer and heat loss coefficients.

To simulate the temperature distribution in the flow direction, we consider the energy balance of the fluid flowing through an element of the collector of length Δx . The useful heat gain as given in Eq. (2) is transferred to the fluid; hence

$$\dot{m}C_p \left((T_{f,x} + \frac{dT_{f,x}}{dx} \cdot \Delta x) - T_{f,x} \right) = \Delta q \cdot b \cdot \Delta x \quad (12)$$

Substituting Δq from Eq. (5) into Eq. (12) gives

$$\frac{\dot{m}C_p}{U_L b F'} \cdot \frac{dT_{f,x}}{dx} = \frac{I}{U_L} - (T_{f,x} - T_a) \quad (13)$$

The above differential equation can be solved using the boundary condition $T_{f,x} = T_{in}$ at $x = 0$, by assuming that F' and U_L are independent of x . The equation then gives

$$T_{f,x} = T_a + \frac{S}{U_L} - \left(\frac{S}{U_L} - (T_{in} - T_a) \right) e^{-\theta x} \quad (14)$$

where

$$\theta = \frac{U_L b F'}{\dot{m}C_p} \quad (15)$$

In the same way as deriving equation for $T_{f,x}$, we can also obtain $T_{p,x}$ and $T_{b,x}$ from Eqs. (4)–(6) and (14). This gives

$$T_{p,x} = T_a + \frac{S}{U'_L} - F' \left(\frac{S}{U'_L} - (T_{in} - T_a) \right) e^{-\theta x} \quad (16)$$

and

$$T_{b,x} = T_a + \frac{S}{U''_L} - \frac{U_L F'}{U''_L} \left(\frac{S}{U'_L} - (T_{in} - T_a) \right) e^{-\theta x} \quad (17)$$

Therefore, for a collector of length L , the outlet fluid temperature is

$$T_{out} = T_a + \frac{S}{U_L} - \left(\frac{S}{U_L} - (T_{in} - T_a) \right) e^{-\theta L} \quad (18)$$

By integrating Eq. (13) from zero to L we obtain the mean air temperature $T_{f,m}$:

$$T_{f,m} = T_a + \frac{S}{U_L} - \frac{F_R}{F'} \left(\frac{S}{U'_L} - (T_{in} - T_a) \right) \quad (19)$$

In the same manner, the mean top plate temperature ($T_{p,m}$) and mean bottom plate temperature ($T_{b,m}$) are obtained as

$$T_{p,m} = T_a + \frac{S}{U'_L} - F_R \left(\frac{S}{U'_L} - (T_{in} - T_a) \right) \quad (20)$$

$$T_{b,m} = T_a + \frac{S}{U''_L} - \frac{U_L F_R}{U''_L} \left(\frac{S}{U'_L} - (T_{in} - T_a) \right) \quad (21)$$

where

$$F_R = \frac{\dot{m}C_p}{AU_L} (1 - e^{-\theta L}) \quad (22)$$

and

$$A = bL \quad (23)$$

The heat loss from the top surface of the collector system takes place mainly by convection and radiation. Since the natural convection is negligibly small compared with the forced convection, the convective heat loss from the top of the collector can be written as

$$q_{conv} = h_w(T_{p,m} - T_a) \quad (24)$$

where

$$h_w = 5.7 + 3.8V \quad (25)$$

for wind speeds slower than 4 m/s [23].

A radiation exchange takes place between the absorber surface at the mean temperature $T_{p,m}$ and the temperature sink composed of the sky and the surroundings, which a tilted collector sees as the mean temperature T_s . For simplicity, T_s is usually replaced by the sky temperature T_{sky} . The radiation heat loss can then be written as

$$q_{rad} = \sigma \epsilon_p h_w (T_{p,m}^4 - T_{sky}^4) \quad (26)$$

The uppercase notation of T represents the temperature in Kelvin. The sky temperature can be expressed as [23]

$$T_{sky} = 0.0552 T_a^{1.5} \quad (27)$$

The top-surface heat loss coefficient can then be derived from Eqs. (24) and (26) and written as

$$U_p = h_w + \sigma \epsilon_p (T_{p,m}^2 + T_{sky}^2)(T_{p,m} + T_{sky}) \left(\frac{T_{p,m} - T_{sky}}{T_{p,m} - T_a} \right) \quad (28)$$

It was investigated that the number of glass covers of a flat-plate solar collector system significantly affects the upward heat loss. A semi-empirical expression proposed in Ref. [23] is

$$U_p = F \left(\left(\frac{N}{\left(\frac{344}{T_{p,m}} \right) \left(\frac{T_{p,m} - T_a}{N + f} \right)^{0.31}} + \frac{1}{h_w} \right)^{-1} + \frac{\sigma (T_{p,m} + T_a)(T_{p,m}^2 - T_a^2)}{(\epsilon_p + 0.0425N(1 - \epsilon_p))^{-1} + \frac{2N + f - 1}{\epsilon_g} - N} \right) \quad (29)$$

The values of f and F are calculated from the following relations:

$$f = (1 - 0.4h_w + 5 \cdot 10^{-4}h_w^2)(1 + 0.056N) \quad (30)$$

$$F = 1 - (S - 45)(0.00259 - 0.00144\epsilon_p) \quad (31)$$

Heat losses from the bottom of the collector are caused mainly by convection and can be minimized by covering the bottom with insulating material. By neglecting the heat loss by radiation, the coefficient heat loss through the bottom can be written as

$$U_b = \left[\frac{1}{h_w} + \sum \frac{l}{k} \right]^{-1} \quad (32)$$

where l is the thickness of the material (m), and k is the conductive heat transfer coefficient of transfer ($\text{W m}^{-2} \text{K}^{-1}$). Here, the collector is considered to be well insulated. Thus, the heat loss from the sides, as well as from the supporting frame, can be neglected.

The coefficient of heat transfer between the absorber and bottom plate inside the flow channel may be evaluated from

$$h_r = \frac{\sigma}{\left(\frac{2}{\epsilon_{p,l}} - 1 \right)} (T_{p,m}^2 + T_{b,m}^2)(T_{p,m} + T_{b,m}) \quad (33)$$

For the convective heat transfer coefficient, a suitable established Nusselt number for evaluating h_p and h_b under the conditions considered herein is not available. Therefore, the empirical equation proposed in Ref. [23] for a fully developed turbulent flow between parallel walls is adopted. The empirical equation for the Nusselt number is written as

$$\text{Nu}_p = 0.0158 \text{Re}^{0.8} \quad (34)$$

3.1.2. Thermal analysis for drying chamber with solar energy

The drying chamber is composed of the trays, wall, base, and roof (glass cover). In the following, equations are constructed for a steady-state situation. Such studies, as described in Ref. [24,25], propose a mathematical model for a similar drying chamber of a solar dryer. The drying rate of the product shelf can be approximately described by a representative average thin layer.

3.1.2.1. Tray 1 (bottom tray). The heat balance on tray 1 of the dryer can be analyzed from following definition: heat convection from the air to the tray + heat convection from the air to the cabinet wall + heat convection from the air to the bottom = sensible

heat loss by the air. Mathematically, this can be written as

$$\begin{aligned} h_{a-p}a_pA_s d_1 \left(\frac{T_1 + T_2}{2} - T_{p1} \right) + h_{a-w}A_{w1} \left(\frac{T_1 + T_2}{2} - T_{w1} \right) + h_{a-b}A_b(T_1 - T_b) \\ = \dot{m}_a \left(C_a + C_v \frac{w_1 + w_2}{2} \right) (T_1 - T_2) \end{aligned} \quad (35)$$

Heat convection from the air to the tray = the enthalpy increase of the air owing to the increase in the moisture content + the net radiation to the bottom, the upper tray, and the cabinet wall:

$$\begin{aligned} h_{a-p}a_pA_s d_1 \left(\frac{T_1 + T_2}{2} - T_{p1} \right) = \dot{m}_a \left(L_e + C_v \frac{T_1 + T_2}{2} - T_1 \right) (w_2 - w_1) \\ + \sigma A_s \left(\frac{T_{p1}^4 - T_b^4}{\frac{1}{\varepsilon_p} + \frac{1}{\varepsilon_b} - 1} \right) + \sigma A_s \left(\frac{T_{p1}^4 - T_{p2}^4}{\frac{1}{\varepsilon_p} + \frac{1}{\varepsilon_t} - 1} \right) + \sigma A_{w1} (\varepsilon_t T_t^4 - \varepsilon_w T_{w1}^4) \end{aligned} \quad (36)$$

For the cabinet wall surrounding the shelf, heat convection from the air to the wall = the conduction loss within the wall + the convection heat loss from the external surface of the wall to the ambient atmosphere:

$$h_{a-w}A_{w1} \left(\frac{T_1 + T_2}{2} - T_{w1} \right) = k_w(T_{w1} - T_{am}) + h_{w-p}(T_{w1} - T_{p1}) \quad (37)$$

For a thin layer that is being dried, the mass exchange within the product and the drying air can be derived from the equation

$$\frac{\partial w}{\partial x} = \frac{\rho_p A_s}{\dot{m}_a} \cdot \frac{\delta M_p}{\delta t} \quad (38)$$

Assuming an average rate $\delta M_1/\delta t$ exists at shelf 1, then

$$w_2 - w_1 = \frac{\rho_p A_s}{\dot{m}_a} \cdot \frac{\delta \overline{M}_{p1}}{\delta t} \quad (39)$$

The quantity of $\delta M_p/\delta t$ can be taken from the thin layer model, which is unique for a particular product [24].

3.1.2.2. Trays 2 and 3. A similar analysis for tray 1 can be applied to trays 2 and 3. Consider a typical tray i of the dryer, where i indicates the tray's number. The energy balance can be analyzed from the following: convection from the air to the shelf + the heat convection from the air to the cabinet wall = sensible heat loss by the air.

$$\begin{aligned} h_{a-p}a_pA_s d_i \left(\frac{T_i + T_{i+1}}{2} - T_{pi} \right) + h_{a-w}A_{wi} \left(\frac{T_i + T_{i+1}}{2} - T_{wi} \right) \\ = \dot{m}_a \left(C_a + C_v \frac{w_i + w_{i+1}}{2} \right) (T_i - T_{i+1}) \end{aligned} \quad (40)$$

Heat convection from the air to the shelf = the enthalpy increase of the air owing to the increase in moisture content + net radiation to other shelves and the cabinet wall:

$$\begin{aligned} h_{a-p}a_pA_s d_i \left(\frac{T_i + T_{i+1}}{2} - T_{pi} \right) = \dot{m}_a \left(L_e + C_v \frac{T_i + T_{i+1}}{2} - T_i \right) (w_{i+1} - w_i) \\ + \sigma A_s \left(\frac{T_{pi}^4 - T_{pi-1}^4}{\frac{1}{\varepsilon_p} + \frac{1}{\varepsilon_t} - 1} \right) + \sigma A_s \left(\frac{T_{pi}^4 - T_{pi+1}^4}{\frac{1}{\varepsilon_p} + \frac{1}{\varepsilon_t} - 1} \right) + \sigma A_{wi} (\varepsilon_t T_t^4 - \varepsilon_w T_{wi}^4) \end{aligned} \quad (41)$$

For the cabinet wall surrounding the shelf: heat convection from the air to the wall = conduction loss within the wall + convection heat loss from the external surface of the wall to the ambient atmosphere:

$$h_{a-w}A_{wi} \left(\frac{T_i + T_{i+1}}{2} - T_{wi} \right) = k_w(T_{wi} - T_{am}) + h_{w-p}(T_{wi} - T_{pi}) \quad (42)$$

The mass exchange within the product and the drying air can be derived from

$$w_{i+1} - w_i = \frac{\rho_p A_s}{\dot{m}_a} \cdot \frac{\delta \overline{M}_{pi}}{\delta t} \quad (43)$$

3.1.2.3. Tray 4. For tray 4 (the top tray), the effects of solar radiation should be included in the heat balance analysis, as the cover of the dryer is made from transparent glass. (Subscript 5 in the following equations indicates the position above tray 4, or just below the roof.) Similar to the other trays, the heat balance equation on tray 4 can be generated from the following definition: heat convection from the air to the tray + heat convection from the air to the cabinet wall + heat convection from the air to the roof = sensible heat

loss by the air.

$$\begin{aligned} h_{a-p}a_pA_s d_4 \left(\frac{T_4 + T_5}{2} - T_5 \right) + h_{a-w}A_{wi} \left(\frac{T_4 + T_5}{2} - T_{w4} \right) + h_{a-r}A_r (T_5 - T_r) \\ = \dot{m}_a \left(C_a + C_v \frac{w_4 + w_5}{2} \right) (T_4 - T_5) \end{aligned} \quad (44)$$

Heat convection from the air to the shelf + solar radiation absorbed = gain in latent heat + net radiation to tray 3, the roof, and the cabinet wall.

$$\begin{aligned} h_{a-p}a_pA_s d_4 \left(\frac{T_4 + T_5}{2} - T_4 \right) + (\tau\alpha)_e A_r G = \dot{m}_a \left(L_e + C_v \frac{T_4 + T_5}{2} - T_4 \right) (w_5 - w_4) \\ + \sigma A_r \left(\frac{T_4^4 - T_r^4}{\frac{1}{\varepsilon_p} + \frac{1}{\varepsilon_r} - 1} \right) + \sigma A_s \left(\frac{T_4^4 - T_3^4}{\frac{1}{\varepsilon_p} + \frac{1}{\varepsilon_i} - 1} \right) + \sigma A_{w4} (\varepsilon_t T_t^4 - \varepsilon_w T_{w4}^4) \end{aligned} \quad (45)$$

For the cabinet wall surrounding the shelf: heat convection from the air to the wall = conduction loss within the wall + convection heat loss from the external surface of the wall to the ambient. Thus,

$$h_{a-w}A_{w4} \left(\frac{T_4 + T_5}{2} - T_{w4} \right) = k_w (T_{w4} - T_{am}) + h_{w-p} (T_{w4} - T_4) \quad (46)$$

For the glass roof, heat convection from the air to the glass roof = heat convection from the roof to the ambient atmosphere + radiation to the sky + net thermal radiation to tray 4. Thus, we find that

$$h_{a-r}A_r (T_5 - T_r) = h_{r-a}A_r (T_r - T_a) + \sigma A_r (T_r^4 - T_{sky}^4) + \sigma A_s \left(\frac{T_r^4 - T_4^4}{\frac{1}{\varepsilon_r} + \frac{1}{\varepsilon_p} - 1} \right) \quad (47)$$

The mass exchange within the product and drying air can be calculated from

$$w_5 - w_4 = \frac{\rho_p A_s}{\dot{m}_a} \cdot \frac{\delta \overline{M}_{p4}}{\delta t} \quad (48)$$

3.1.3. Numerical simulation

The set of Eqs. (1)–(31) above was solved to identify the output temperature of the solar collector, and the set Eqs. (35)–(48) to predict the air temperatures on the trays. Computations were made by creating a simple computer program using MATLAB. In the calculation procedure, the collector was divided into a finite number of elements/segments over which the heat loss and heat transfer coefficients were constant. The computation was started with given initial values of UL, UL', and UL'' and for the first segment of the collector. The material properties constants were taken from the literature [23]. The drying parameters over a range of temperatures for each tray were considered separately. In the solar drying process, most of the drying parameters (such as solar radiation, relative humidity, ambient temperature, and wind velocity) are not steady.

3.2. Simulation with FloVent

In addition to numerical simulation, a Computational Fluid Dynamics (CFD) simulation was run using the FloVent program to predict the temperature distribution and air flow pattern in the drying chamber, especially for the situation when the back-up heater (biomass burner) has to operate. The FLOVENT program uses CDF techniques to predict the airflow, heat transfer and contamination control within a room or a building [20]. The complex effects of air viscosity, buoyancy and turbulence are properly represented so that a detailed and accurate picture of both the air distribution and the consequent heat transfer process can be obtained.

The mathematical simulation of fluid flow and heat transfer phenomena involves the solution of a set of coupled, non-linear, second order partial differential equations, which describe the conservation of mass, momentum and energy. By setting the boundary conditions, the resulting flow and temperature patterns are determined by solving these equations all together.

The governing equations, based on the Reynolds-averaged Navier-Stokes (*Re k-ε*) model for natural convection flows [21], are given by: Continuity equation

$$\frac{\partial}{\partial x_i} (\rho \overline{u}_i) = 0 \quad (49)$$

Averaged Navier-Stokes equations

$$\frac{\partial}{\partial x_i} (\rho \overline{u}_j \overline{u}_i) = -\frac{\partial \overline{P}}{\partial x_i} + \frac{\partial}{\partial x_j} \left[\mu \left(\frac{\partial \overline{u}_i}{\partial x_j} + \frac{\partial \overline{u}_j}{\partial x_i} \right) - \rho \overline{u'_i u'_j} \right] - \rho g_i \beta (\overline{T} - \overline{T}_{ref}) \quad (50)$$

Energy equation

$$\frac{\partial}{\partial x_i}(\rho \bar{u}_i \bar{T}) = \frac{\partial}{\partial x_i} \left[\frac{\mu}{Pr} \frac{\partial \bar{T}}{\partial x_i} - \rho \bar{u}_i' \bar{T}' \right] \quad (51)$$

Where, \bar{u} is the mean velocity components (u, v, w), \bar{u}_i' is the velocity fluctuation and \bar{P} is the pressure. Here, x_i is the coordinate axis (x, y, z), ρ is the density, g_i is the gravitational acceleration vector and β is the thermal expansion coefficient. The diffusion term is indicated by viscosity μ . The Boussinesq approximation is employed in the last term of Eq. (5.50). Where $T_{ref} = \frac{1}{2}(T_h + T_c)$ is the reference temperature, \bar{T} is the mean temperature, and \bar{T}' is the temperature fluctuation.

The averaging process results in two new unknowns, $-\rho \bar{u}_i' \bar{u}_j'$ and $-\rho \bar{u}_i' \bar{T}'$, called Reynolds terms. The first term is called the Reynolds stress (τ_{ij}). The latter can be considered as a diffusion term for the enthalpy. The determination of the Reynolds terms requires extra equations. The correlation of the Reynolds terms to the mean flow field is resolved by turbulence models. The turbulent stresses are proportional to the mean velocity gradients:

$$\tau_{ij} = -\rho \bar{u}_i' \bar{u}_j' = \mu_t \left(\frac{\partial \bar{u}_i}{\partial x_j} + \frac{\partial \bar{u}_j}{\partial x_i} \right) - \frac{2}{3} \delta_{ij} \rho k \quad (52)$$

$$-\rho \bar{u}_i' \bar{T}' = \Gamma_t \frac{\partial \bar{T}}{\partial x_i} \quad (53)$$

Where μ_t is the turbulent or eddy viscosity, a property of the flow, Γ_t the turbulent scalar diffusivity (also given as μ_t/σ_H , where σ_H is the turbulent-Prandtl number), δ_{ij} the Kronecker delta, and k is the turbulent kinetic energy.

In the CFD technique used in FloVent, the conservation equations are discretized by sub-division of the domain of integration into a set of non-overlapping, contiguous finite volumes over each of which the conservation laws are expressed in algebraic form. These finite volumes are referred to as grid cells. The discretization results in a set of algebraic equations, each of which relates to the value of variable in a cell to its value in the nearest -neighbor grid cells. The summary of the algorithm used in FloVent for a 3D simulation of flow and heat transfer can be defined as follow:

- initialize the first of pressure, temperature and velocities,
- increase outer iteration by 1,
- set up coefficients for temperature field, T ,
- solve linearized algebraic equations for the value of T in each cell by performing a number of inner iterations
- repeat steps c and d for field variables of u, v, w, k and ϵ
- solve the continuity equations in similar manner and make any associated adjustments to pressure and velocities,
- check for convergence and return to step b if required.

3.2.1. Experiments with the dryer

A series of experiments with the dryer was carried out, and the results are compared with those of the simulations. Forced convection tests were carried out to investigate the performance of the solar collector. For this purpose, a centrifugal blower was applied to generate air at a certain mass flow rate. The suction blower, which was positioned at the left side of the ventilation of the dryer, sucked the air out of the chamber. The air mass flow rate was measured with an anemometer. A combination of handheld instruments and sensors connected to a data logger (DataTaker 605) was used to record the measurements. The temperature and solar radiation were recorded every 10 min. The solar radiation was measured with a pyranometer (Kipp & Zonen CM 3) with a sensitivity of $16.51 \times 10^{-6} \text{ V/Wm}^{-2}$ and an accuracy of $\pm 5\%$.

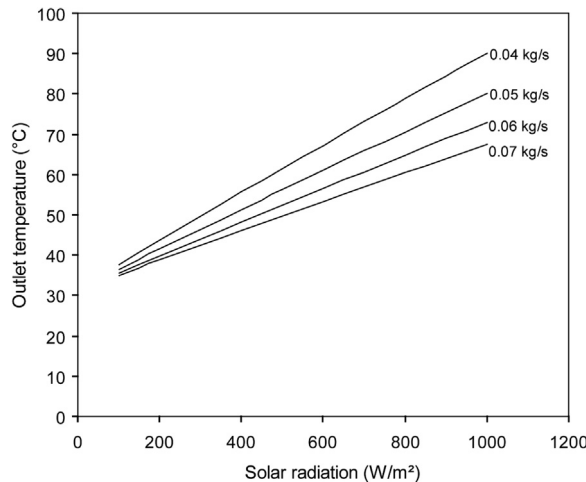


Fig. 3. Outlet air temperature of solar collector for different air mass flow rates with single glass cover and thickness of back insulator = 3 cm.

Preliminary tests indicated that the temperature profile across the width of the collector was uniform. In the test, therefore, the temperature was measured just in the centerline along the length of the collector at three points. The measurement points were located at 10 cm from the inlet side, at the center, and at 10 cm from outlet side of the collector. The temperature measurements were also measured at the bottom plate, in the air stream, and at the absorber plate.

For the drying chamber, serial tests for unloaded dryer conditions were conducted. A performance evaluation was made by varying the ratio of the energy source, i.e., including solar energy and biomass (firewood) back-up heating with heat storage.

4. Results and discussion

4.1. Solar collector

Fig. 3 shows the results of the simulation on the outlet air temperature from the solar collector as a function of the solar radiation for different values of the air mass flow rate, which varied from 0.04 to 0.07 kg/s⁻¹. This range of values was reported for flat plate types of solar air heater in the literature. The simulation results showed that with conditions of air mass flow rate = 0.06 kg/s, a single glass cover, thickness of back insulator = 3 cm, and $h_w = 9.5 \text{ W/m}^2 \text{ K}^{-1}$, the outlet air temperature reached 60 °C at a solar radiation of 750 W/m².

The presence of a glass cover significantly increases the temperature of the collector, as shown in Fig. 4. However, increasing the number of glass covers (N) from 1 to 2 does not significantly affect the temperature. Varying the thickness of the back insulation has negligible effects, especially for thicknesses over 3 cm, as shown in Fig. 5.

4.2. Comparison of simulation and experimental results

The simulation and experimental results of the solar collector system showed good agreement. The experimental and simulation results on the outlet air temperatures of the collector as a function of global solar radiation are compared in Figs. 6 and 7 at air flow rates of 0.052 and 0.062 kg/s, respectively.

Fig. 8 shows the experimental and simulation results on the temperature distribution of the absorber plate as functions of the global solar radiation. During the experiment, the maximum temperature of the absorber plate was found to be 110 °C at a solar radiation of 1000 W/m². For the range of high solar radiation, the experimental results showed a lower temperature than that of the simulation. This was probably caused by heat loss, which is affected by many factors of the surroundings, as the real conditions are higher than the predicted values.

With an air mass flow rate of about 0.052 kg/s, both the experimental and simulation results show that the outlet air temperature reaches 60 °C at a solar radiation of about 550 W/m². The outlet air temperatures significantly decrease with an increasing air mass flow rate. With an air mass flow rate of 0.062 kg/s and solar radiation of 550 W/m², the outlet air temperature was reduced to 53 °C.

The results from the experiment show that the outlet air temperatures with forced convection are significantly higher than those from natural convection. The maximum temperature that can be reached with forced convection with an air mass flow rate of 0.062 kg/s was about 71 °C when the solar radiation was about 950 W/m². By contrast, with natural convection, the maximum temperature of the outlet air was about 61 °C.

4.3. Drying chamber

The main purpose of the simulation was to predict the dryer performance in order to optimize the design. In all simulation runs, the material property constants were taken from the literature [23]. The inlet air to the drying chamber is the outlet air from the solar

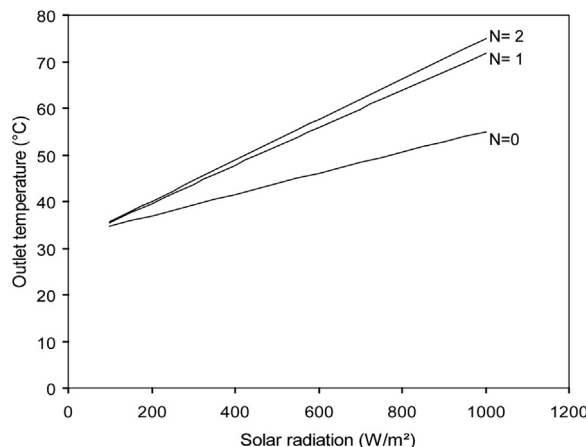


Fig. 4. Effect of number of glass cover sheets on temperature of outlet air.

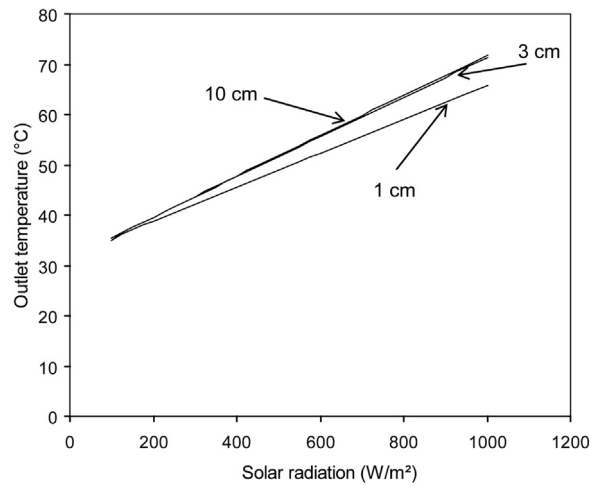


Fig. 5. Effect of insulation thickness on temperature of outlet air.

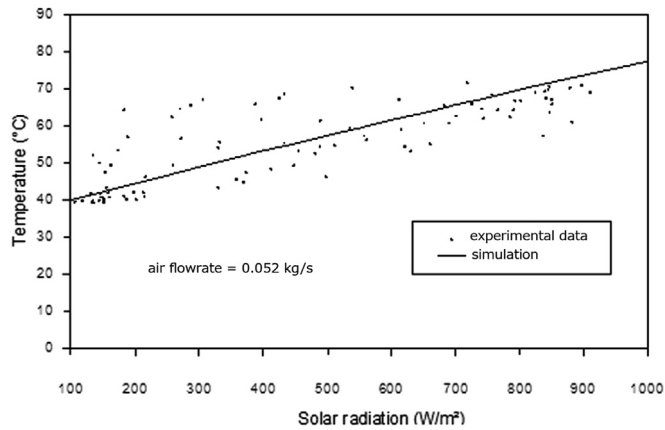


Fig. 6. Comparison of experimental and predicted results for temperature distribution of outlet air of solar collector with air flow rate of 0.052 kg/s.

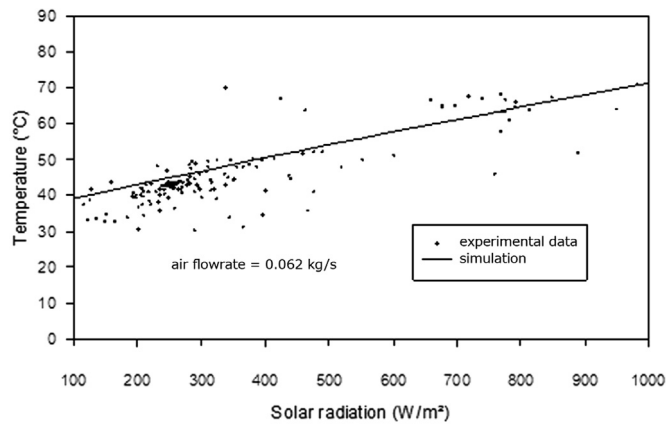


Fig. 7. Comparison of experimental and predicted results for temperature distribution of outlet air of solar collector with air flow rate of 0.062 kg/s.

collector. For computational simplification, the air flow rate is assumed to be constant at 0.062 kg/s. This value is taken from the average values commonly reported in the literature for the same type of solar dryer [3,22,24], and recalculated according to the dryer size. A simulation with an empty dryer was conducted by setting the humidity ratio on each tray at a constant value.

The simulation results for the air temperature with empty trays (no load) as a function of solar radiation are shown in Fig. 9.

As shown in Fig. 9, there is a small difference in temperature between the first three trays: the highest temperature is on tray 3,

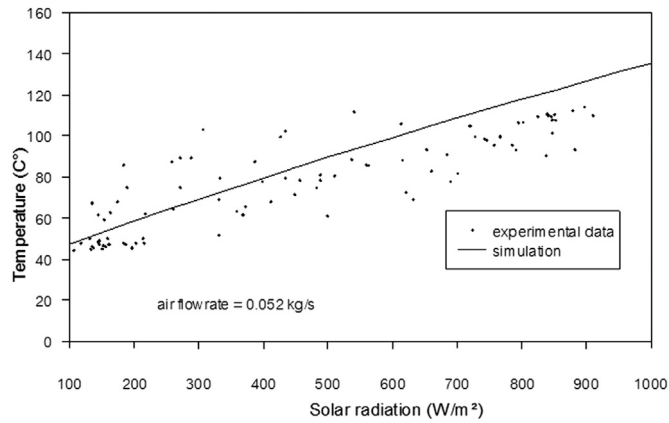


Fig. 8. Comparison of experimental and predicted results for temperatures distribution of absorber plate.

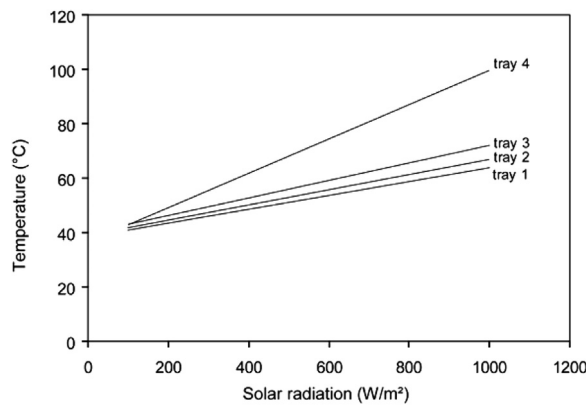


Fig. 9. Simulation results of air temperature on each tray of dryer as function of solar radiation.

followed by tray 2 and then tray 1. The temperature on tray 4 is significantly higher than the temperatures on the other three trays. This is because tray 4 receives additional heat from direct solar radiation through the transparent (glass) cover on the top of the drying chamber. However, the temperature of each tray will decrease if it is loaded during the drying of products.

The simulation and experimental results for the air temperature on each tray are shown in Figs. 10 and 11, respectively. The process was simulated from 8:30 a.m. to 5:00 p.m. The simulation results showed good agreement with the experimental results. The input solar radiation and ambient temperature for the simulation were taken from real data for the experiment.

The maximum air temperatures were about 65°, 58°, 48°, and 45° on tray 4, tray 3, tray 2, and tray 1, respectively, owing to a solar radiation of about 1000 W/m². In most cases, the maximal temperature coincides with the maximal solar radiation. During the

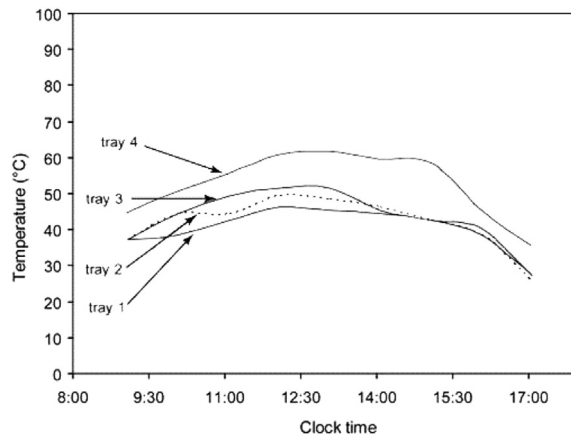


Fig. 10. Simulation results for temperature of air on each dryer tray.

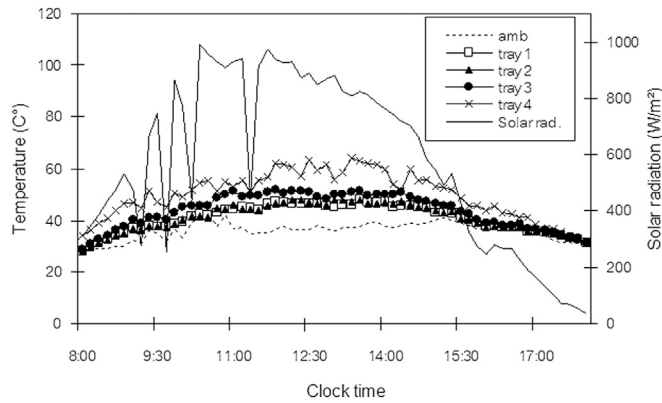


Fig. 11. Experimental results for distribution of air temperatures on each tray.

experiment, it was identified that the low and fluctuating solar radiation owing to moving clouds significantly affects the air temperatures in the drying chamber.

A preliminary test for the solar dryer was carried out to evaluate the moisture and drying kinetics for different trays. The experiment was conducted for 24 h, with a loading of 110-kg coffee cherries. This load is about full capacity of the dryer. The experiment was started with back-up heater system mode by firewood burning (started at 18.00), and continued with solar energy mode during day time on the next day. About 75 kg of wood with 48% (d.b.) moisture content was burned in one time feeding. The decrease of the moisture content of the product during the first 24 h of drying process is shown in Fig. 12. The products on tray one obviously dry fastest. The moisture content was reduced from 180% to 50% (d.b.), while the moisture content of the product on the other three trays was reduced to about 58%.

4.3.1. CFD simulation

A simulation was performed using FloVent 5.2 for the back-up heater (biomass burner) operation. In the simulation, the model was simplified so that the bricks (heat storage) at the bottom and the walls of the drying chamber (excluding the doors) were assumed to be the heat source components. Owing to the limitations of the simulation program, the simulation was conducted mainly for an empty room. However, a perforated plane was set to represent each tray in the dryer.

A preliminary experiment on the designed dryer indicated that the temperature of the brick at the top level (the brick that is in contact with the drying chamber) can be sustained at an average value of about 250 °C for more than 7 h, while the temperature of the wall is about 110 °C. These values were set as the boundary conditions in the simulation.

Fig. 13(a) and (b) show the temperature contours for the cross section of the chamber from the side and from the front, respectively. With the conditions as simulated, the average drying air temperature in the drying chamber was found to be 56 °C. This value is suitable for the drying of agricultural products. There was a small temperature difference between the trays. However, the temperature was found to be uniform across each tray. The effect of the mesh on the trays was not studied in this work, and this might be attempted for further improvement of the model.

Fig. 13(a) and (b) show that the highest temperature occurs at the bottom edge and wall of the drying chamber. This is because the bottom plate is near (in contact with) the heat source. The lowest temperatures are found just below tray 1, which is probably

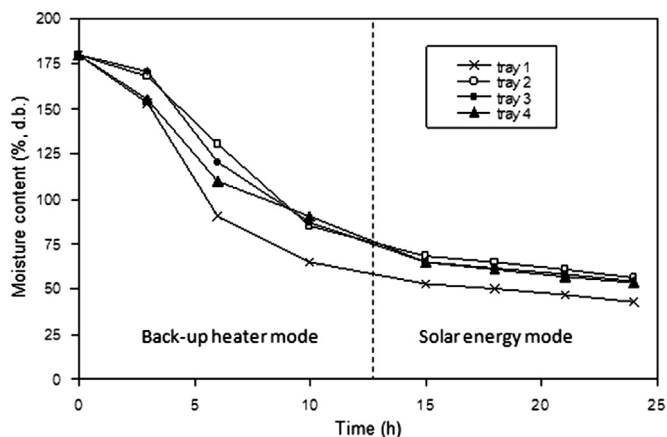


Fig. 12. The decrease of moisture content of coffee cherries during with different modes of drying.

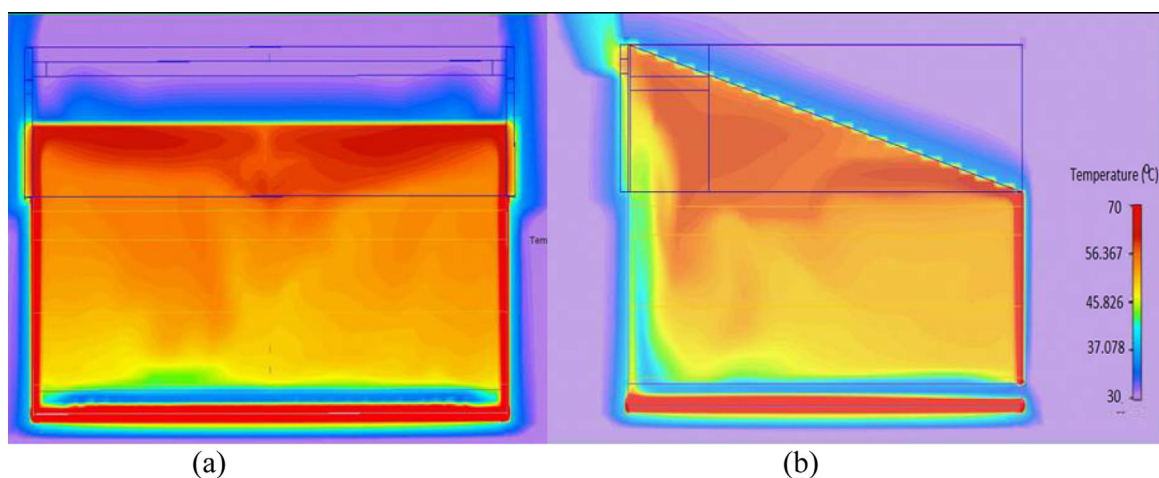


Fig. 13. CFD simulation of temperature distribution of air in drying chamber: (a) front view and (b) side view.

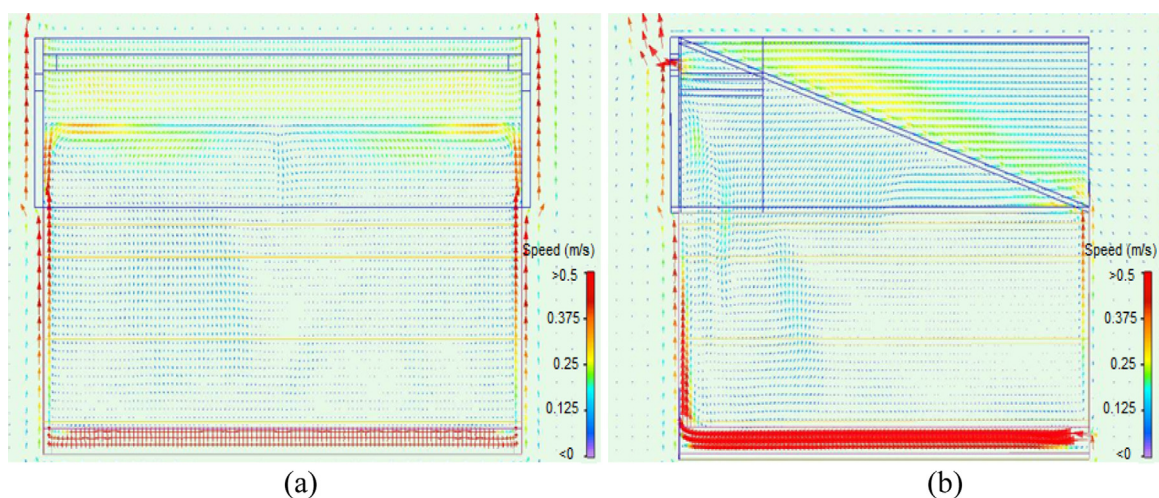


Fig. 14. Air speed distribution in drying chamber: (a) front view and (b) side view.

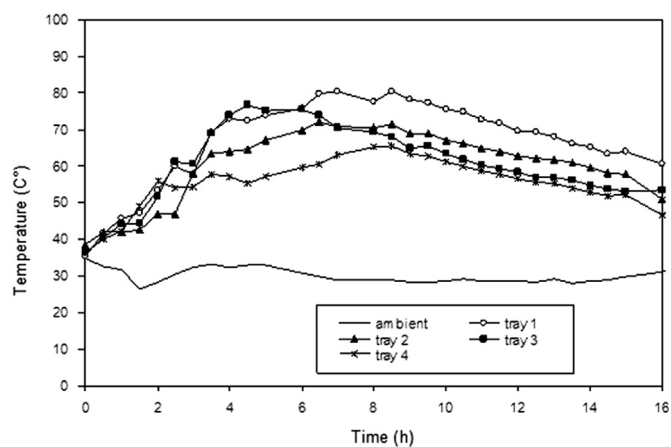


Fig. 15. Distribution of air temperature on each tray for the dryer operation with biomass burner and heat storage.

owing to the space in the path of the flow of the fresh air to the chamber. This is confirmed with high velocity as shown by air speed contours in Fig. 14. In general, the average air velocity was found to be 0.13 m/s in all directions.

4.3.2. Biomass back-up heater experiment results

When the back-up heater burner was used, the air temperature on the trays gradually increases and reaches a maximum value after about five hours from the start of wood burning as shown in Figure 6.12. This slow increase of the temperature indicates that a part of the heat from combustion was stored in the bricks when the exhaust gas and hot smoke passes through them. By burning about 75 kg of woods, the combustion could be sustained for about 4 h without adding more firewood. Using large pieces and slow burning hardwood causes the fire to burn more slowly and last longer.

Figure 6.12 shows the temperature distribution on the dryer trays during the first 14 h of the test, when burning 70 kg wood. The maximum temperature that was achieved on tray two, three, and four was 71, 73, and 61 °C, respectively. For tray 1, the maximum temperature was 80 °C, which is too high for drying most types of agricultural products. However, when the trays are loaded with any product to be dried, the air temperature is certainly lower. The high temperature on tray 1 is probably due to the position of the tray close to bottom plate, which is placed directly on the top surface of bricks (heat storage). Supplying the burner with less than 75 kg wood can reduce the maximum temperature on the trays. Another experiment with burning of 60 kg of similar wood proved that the maximum temperature on the trays 4 was indeed reduced, even to 65 °C, and thus was suitable for drying most the agricultural products. However, a reduction of wood would reduce stored heat too. This was indicated by a fast decrease in temperature after the maximum value had been reached.

When the combustion in the burner was over, the stored heat in the bricks obviously started to contribute to the drying air. The temperature still gradually increased for a few hours and then decreased. When the test was started in the evening at 18.00 by supplying 70 kg of fuel woods, the temperatures on the trays in the morning of the next day remained 60, 53, 50, and 49 °C for tray one, two, three, and four, respectively, with an ambient temperature of 29 °C (Fig. 15). In this case, for the second day, the source of heat would be from both solar energy and stored heat in the brick. The bricks still continue supplying heat until midnight in the second day, and keep the temperature on tray 18 °C above the ambient temperature of about 25 °C. Again, this shows that the biomass burner and heat storage facility do indeed can improve the viability of solar dryer.

Comparing with CFD simulation for the back-up heater system, where all parameters inputs and boundary conditions are constant values and under ideal condition, it might be difficult to validate it by a real experiment. However, the simulation results would be useful for predicting the dryer performance prior to the real construction. In general, the CFD simulation results has a good agreement with the experiment results in term of temperature in the drying chamber (Fig. 12), particularly when a steady state had been reached i.e., after around eight hours of burning wood in the experiment (Fig. 15).

5. Conclusion

The mathematical modeling and simulation of a solar agricultural dryer with back-up biomass burner and thermal storage was performed. Results from the simulation of the outlet air temperature from the solar collector show that the presence of a glass cover significantly increases the temperature of the collector. However, increasing the number of glass covers from one to two does not significantly affect the temperature. Varying the thickness of the back insulation has negligible effects, especially for thicknesses over 3 cm. The simulation result with unloaded trays of the dryer shows that there is a small difference in temperature between the bottom three trays, while the temperature on the top tray is significantly higher. This is because the top tray receives additional heat from direct solar radiation.

The temperature distribution and air flow pattern in the drying chamber with a back-up biomass burner were accomplished by the Computational Fluid Dynamics method. The results show an average drying air temperature in the drying chamber of 56 °C. This value is suitable for the drying of agricultural products. Temperature differences between the trays and across each tray were found to be small. With regard to the simulation results, in general, it can be concluded that the simulated dryer conditions are appropriate for drying agricultural products.

References

- [1] A.A. El-Sebaii, S.M. Shalaby, Solar drying of agricultural products: a review, *Renew. Sustain. Energy Rev.* 16 (1) (2012) 37–43.
- [2] E. Tarigan and P. Tekasakul, A Small Scale Solar Agricultural Dryer with Biomass Burner and Heat Storage Back-Up Heater. in: *Proceedings of the ISES World Congress 2007 (Vol. I – Vol. V)*, Berlin, Heidelberg: Springer Berlin Heidelberg, 2008, pp. 1956–1959.
- [3] B.K. Bala, J.L. Woods, Optimization of natural-convection, solar drying systems, *Energy* 20 (4) (. 1995) 285–294.
- [4] M.E.A. Slimani, M. Amirat, S. Bahria, I. Kurucz, M. Aouli, R. Sellami, Study and modeling of energy performance of a hybrid photovoltaic/thermal solar collector: configuration suitable for an indirect solar dryer, *Energy Convers. Manag.* 125 (2016) 209–221.
- [5] G. Duran, M. Condori, F. Altobelli, Simulation of a passive solar dryer to charqui production using temperature and pressure networks, *Sol. Energy* 119 (2015) 310–318.
- [6] Simate, Optimization of mixed-mode and indirect-mode natural convection solar dryers, *Fuel Energy Abstr.* 44 (4) (. 2003) 236.
- [7] A. El Khadraoui, S. Bouadila, S. Kooli, A. Farhat, A. Guizani, Thermal behavior of indirect solar dryer: nocturnal usage of solar air collector with PCM, *J. Clean. Prod.* 148 (2017) 37–48.
- [8] R. Daghighi, A. Shafieian, An experimental study of a heat pipe evacuated tube solar dryer with heat recovery system, *Renew. Energy* 96 (2016) 872–880.
- [9] L. Bennamoun, A. Belhamri, Mathematical description of heat and mass transfer during deep bed drying: effect of product shrinkage on bed porosity, *Appl. Therm. Eng.* 28 (17) (2008) 2236–2244.
- [10] A. Bahnasawy, M. Shenana, A mathematical model of direct sun and solar drying of some fermented dairy products (Kishk), *J. Food Eng.* 61 (3) (2004) 309–319.
- [11] M. Hasan, T.A.G. Langrish, Development of a sustainable methodology for life-cycle performance evaluation of solar dryers, *Sol. Energy* 135 (2016) 1–13.

- [12] M.M. Morad, M.A. El-Shazly, K.I. Wasfy, H.A.M. El-Maghawry, Thermal analysis and performance evaluation of a solar tunnel greenhouse dryer for drying peppermint plants, *Renew. Energy* 101 (2017) 992–1004.
- [13] D.K. Rabha, P. Muthukumar, C. Somayaji, Experimental investigation of thin layer drying kinetics of ghost chilli pepper (*Capsicum chinense* Jacq.) dried in a forced convection solar tunnel dryer, *Renew. Energy* 105 (2017) 583–589.
- [14] M. Kumar, S.K. Sansaniwal, P. Khatak, Progress in solar dryers for drying various commodities, *Renew. Sustain. Energy Rev.* 55 (2016) 346–360.
- [15] S. Sonthikun, P. Chairat, K. Fardsin, P. Kirirat, A. Kumar, P. Tekasakul, Computational fluid dynamic analysis of innovative design of solar-biomass hybrid dryer: an experimental validation, *Renew. Energy* 92 (2016) 185–191.
- [16] A.E. Kabeel, M. Abdelgaied, *Performance of novel solar dryer*, 2016.
- [17] T.A. Yassen, H.H. Al-Kayiem, Experimental investigation and evaluation of hybrid solar/thermal dryer combined with supplementary recovery dryer, *Sol. Energy* 134 (2016) 284–293.
- [18] E. Tarigan, G. Prateepchaikul, R. Yamsaengsung, A. Sirichote, P. Tekasakul, Sorption isotherms of shelled and unshelled kernels of candle nuts, *J. Food Eng.* 75 (4) (2006) 447–452.
- [19] E. Tarigan, G. Prateepchaikul, R. Yamsaengsung, A. Sirichote, P. Tekasakul, Drying characteristics of unshelled kernels of candle nuts, *J. Food Eng.* 79 (3) (2007) 828–833.
- [20] <https://www.mentor.com>, FloVENT Overview - Mentor Graphics. [Online]. Available: <<https://www.mentor.com/products/mechanical/resources/overview/flovent-overview-1bddfae8-40ef-4ed0-aa7a-59f1351a17d3>>. (Accessed 17 Febuary 2017).
- [21] M. Promtong, P. Tekasakul, CFD study of flow in natural rubber smoking-room: i. Validation with the present smoking-room, *Appl. Therm. Eng.* 27 (11) (2007) 2113–2121.
- [22] K.S. Ong, Thermal performance of solar air heaters: mathematical model and solution procedure, *Sol. Energy* 55 (2) (. 1995) 93–109.
- [23] J.A. Duffie, W.A. Beckman, *Solar Engineering of Thermal Processes*, Wiley, 2013.
- [24] V.K. Sharma, S. Sharma, H.P. Garg, Mathematical modelling and experimental evaluation of a natural convection type solar cabinet dryer, *Energy Convers. Manag.* 31 (1) (1991) 65–73.
- [25] S. Chirarattananon, C. Chinporncharoenpong, R. Chirarattananon, A steady-state model for the forced convection solar cabinet dryer, *Sol. Energy* 41 (4) (1988) 349–360.

also developed by scimago:



SCIMAGO INSTITUTIONS RANKINGS

SJR

Scimago Journal & Country Rank

Enter Journal Title, ISSN or Publisher Name

[Home](#)[Journal Rankings](#)[Country Rankings](#)[Viz Tools](#)[Help](#)[About Us](#)

Case Studies in Thermal Engineering

Country [United Kingdom](#) - [SJR Ranking of United Kingdom](#)

16

H Index

Subject Area and Category [Chemical Engineering](#)
[Fluid Flow and Transfer Processes](#)[Engineering](#)
[Engineering \(miscellaneous\)](#)**Publisher** [Elsevier BV](#)**Publication type** Journals**ISSN** 2214157X**Coverage** 2013-ongoing[Join the conversation about this journal](#)

Quartiles



Engineering (miscellaneous)

Fluid Flow and Transfer Processes

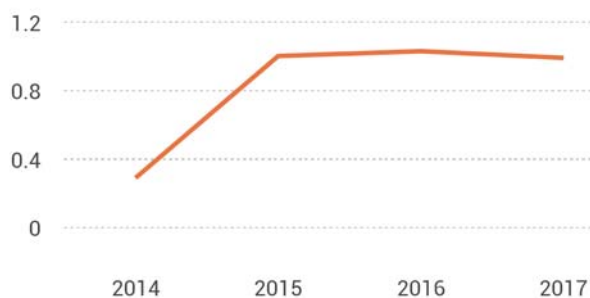
2014

2015

2016

2017

● SJR



● Total Cites ● Self-Cites



500

Citations per document

